Cell Death and Differentiation (2015) 22, 986–999

www.nature.com/cdd

MicroRNA-221 inhibits autophagy and promotes heart failure by modulating the p27/CDK2/mTOR axis

M Su[1,5], J Wang[1,5], C Wang[1,5], X Wang[1], W Dong[2], W Qiu[3], Y Wang[1], X Zhao[4], Y Zou[1], L Song[1], L Zhang*[,2] and R Hui*[,1]

MicroRNAs have emerged as crucial regulators of cardiac homeostasis and remodeling in various cardiovascular diseases. We previously demonstrated that miR-221 regulated cardiac hypertrophy *in vitro*. In the present study, we demonstrated that the cardiac-specific overexpression of miR-221 in mice evoked cardiac dysfunction and heart failure. The lipidated form of microtubule-associated protein 1 light chain 3 was significantly decreased and sequestosome 1 was accumulated in cardiac tissues of transgenic (TG) mice, indicating that autophagy was impaired. Overexpression of miR-221 *in vitro* reduced autophagic flux through inhibiting autophagic vesicle formation. Furthermore, mammalian target of rapamycin (mTOR) was activated by miR-221, both *in vivo* and *in vitro*. The inactivation of mTOR abolished the miR-221-induced inhibition of autophagy and cardiac remodeling. Our previous study has demonstrated that cyclin-dependent kinase (CDK) inhibitor p27 was a direct target of miR-221 in cardiomyocytes. Consistently, the expression of p27 was markedly suppressed in the myocardia of TG mice. Knockdown of p27 by siRNAs was sufficient to mimic the effects of miR-221 overexpression on mTOR activation and autophagy inhibition, whereas overexpression of p27 rescued miR-221-induced autophagic flux impairment. Inhibition of CDK2 restored the impaired autophagic flux and rescued the cardiac remodeling induced by either p27 knockdown or miR-221 overexpression. These findings reveal that miR-221 is an important regulator of autophagy balance and cardiac remodeling by modulating the p27/CDK2/mTOR axis, and implicate miR-221 as a therapeutic target in heart failure.
Cell Death and Differentiation (2015) **22,** 986–999; doi:10.1038/cdd.2014.187; published online 14 November 2014

Heart failure is the ultimate outcome of various cardiovascular diseases and is a leading cause of morbidity and mortality worldwide. Although drugs and other therapies have been developed for the management of heart failure, its 5-year mortality rate remains high.[1] In response to myocardial stresses, the heart initially compensates with cardiomyocyte hypertrophy. Under prolonged stress, the heart undergoes irreversible cardiac remodeling, which finally results in cardiac decompensation and subsequent heart failure. The process of pathological cardiac remodeling involves the dysregulation of many coding and non-coding genes; however, not all of these genes have been well characterized.

MicroRNAs (miRNAs) are endogenous small non-coding RNA molecules that posttranscriptionally regulate the degradation and/or translation of their target genes.[2] A large body of evidence indicates that miRNA-mediated gene regulation has important roles in the control of cardiac homeostasis and pathological remodeling.[3–8] We previously found that miR-221 is significantly upregulated in patients with hypertrophic cardiomyopathy (HCM) and in a mouse model of cardiac hypertrophy and heart failure induced by pressure overload. The *in vitro* overexpression of miR-221 alone is sufficient to increase the size of cardiomyocytes, accompanied by enhanced expression levels of atrial natriuretic polypeptide (ANP) and brain natriuretic peptide (BNP).[9] However, the *in vivo* roles and molecular mechanisms of miR-221 in the regulation of cardiac remodeling remain unclear.

Autophagy is a highly regulated process for bulk degradation, through which cytosolic proteins and organelles are sequestered into autophagosomes and subsequently degraded by lysosomes.[10] Autophagy is required to remove damaged organelles and protein aggregates to maintain

[1]State Key Laboratory of Cardiovascular Disease, Sino-German Laboratory for Molecular Medicine, Fuwai Hospital, National Center for Cardiovascular Disease, Chinese Academy of Medical Sciences and Peking Union Medical College, Beijing 100037, China; [2]Key Laboratory of Human Diseases Comparative Medicine, Ministry of Health, Institute of Laboratory Animal Science, Chinese Academy of Medical Sciences and Peking Union Medical College, Beijing 100021, China; [3]Department of Urology, Peking University First Hospital and the Institute of Urology, Beijing 100034, China and [4]Department of Cardiology, Qingdao Municipal Hospital, Qingdao University, Qingdao 266071, China

*Corresponding author: R Hui, State Key Laboratory of Cardiovascular Disease, Sino-German Laboratory for Molecular Medicine, Fuwai Hospital, National Center for Cardiovascular Disease, Chinese Academy of Medical Sciences and Peking Union Medical College, 167 Beilishilu, Beijing 100037, China. Tel: +86 10 88398154; Fax: +86 10 68331730; E-mail: huirutai@gmail.com

or L Zhang, Key Laboratory of Human Diseases Comparative Medicine, Ministry of Health, Institute of Laboratory Animal Science, Chinese Academy of Medical Sciences and Peking Union Medical College, No. 5, Panjiayuannanli, Chaoyang District, Beijing 100021, China. Tel: +86 10 87778442; Fax: +86 10 67776394; E-mail: zhanglf@cnilas.org

[5]These authors contributed equally to this work.

Abbreviations: miRNA (miR), microRNA; mTOR, mammalian target of rapamycin; Raptor, regulatory-associated protein of mTOR; CDK2, cyclin-dependent kinase 2; LC3, microtubule-associated protein 1 light chain 3; p62, sequestosome 1; ANP, atrial natriuretic polypeptide; BNP, brain natriuretic peptide; PBS, phosphate-buffered saline; α-MHC, α-myosin heavy chain; GFP, green fluorescent protein; mRFP, monomeric red fluorescent protein; TUNEL, terminal deoxynucleotidyltransferase dUTP nick end-labeling; Tg, transgenic; NTG, non-TG; LVIDd, internal dimension of left ventricular at diastole; LVIDs, internal dimension of left ventricular at systole; LVPWd, left ventricular posterior wall at diastole; LVPWs, left ventricular posterior wall at systole; LVAWd, left ventricular anterior wall at diastole; LVAWs, left ventricular anterior wall at systole; LV Mass, left ventricular mass; LV Mass/BW, ratios of LV Mass/body weight; FS, fractional shortening

Received 14.3.14; revised 20.8.14; accepted 09.10.14; Edited by H-U Simon; published online 14.11.14

cellular function and protein quality.[10,11] The cardiomyocyte-specific abrogation of basal autophagy that results from an Atg5 deficiency leads to spontaneous cardiac hypertrophy.[12,13] Under stress stimulation, autophagy acts either as a protective mechanism that promotes cardiomyocyte survival or as a maladaptive mechanism that induces cell death, depending on the context of the stress.[14,15] The activation of autophagy during stress conditions, such as myocardial ischemia and pressure overload, is generally an adaptive response to compensate for energy loss and to remove damaged mitochondria and protein aggregates.[16] However, exaggerated autophagic activity can result in the excessive degradation of organelles and, eventually, cell death.[15] The suppression of autophagy through the down-regulation of Beclin-1 protects the heart from myocardial injuries due to ischemia reperfusion.[14] Therefore, a level of autophagic activity either above or below the basal range may be maladaptive for cardiac homeostasis and cardiac function. However, the mechanisms that regulate autophagy in cardiomyocytes are still poorly understood.

In the present study, we found that the cardiac-specific overexpression of miR-221 in mice evoked cardiac dysfunction and heart failure. These consequences resulted from the inhibition of autophagy induced by miR-221. Moreover, we demonstrated that miR-221 regulated autophagy in cardiomyocytes and cardiac remodeling by modulating cyclin-dependent kinase (CDK) inhibitor p27/CDK2/mammalian target of rapamycin (mTOR), a previous unknown signaling axis.

Results

Overexpression of miR-221 induces heart failure in transgenic mice. To investigate whether miR-221 regulates cardiac remodeling *in vivo*, we generated transgenic (TG) mice (Tg-miR-221) with cardiac-specific overexpression of miR-221, driven by the *α*-myosin heavy chain (*α*-MHC) promoter. Compared with their non-TG (NTG) littermates, Tg-miR-221 mice had significantly higher expression levels of miR-221 in the heart but not in other organs, including the lung, liver, kidney, skeletal muscle, and aorta (Figure 1a). In addition, the expression levels of miR-222, which belongs to the same cluster as miR-221, were not altered by the overexpression of miR-221 (Supplementary Figure S1).

The hearts of the Tg-miR-221 mice were significantly enlarged at 4 weeks of age (Figures 1b and c). The heart-to-body weight ratios (Figure 1d) and the expression levels of ANP and BNP (Figure 1e) were significantly higher in Tg-miR-221 mice than in their NTG littermates. Increased interstitial fibrosis (Figures 1f and g) and apoptosis (Figures 1h and i) were observed in the myocardia from Tg-miR-221 mice by histological examination. Cardiac function was evaluated by using high-resolution echocardiography at 4 and 16 weeks of age. Compared with their age-matched NTG controls, Tg-miR-221 mice exhibited a progressive thickening of the end-diastolic left ventricular posterior wall, an increased internal dimension of the left ventricle and left ventricular mass/body weight ratio, and decreased fractional shortening (Figures 1j and n and Supplementary Table S1). Taken together, these results indicated that the overexpression of miR-221 interrupted cardiac homeostasis and induced cardiac dysfunction and heart failure in mice.

MiR-221 inhibits autophagy, both *in vivo* and *in vitro*. We further analyzed the ultrastructure of the myocardia by using transmission electron microscopy. In cardiomyocytes from NTG mice, the mitochondria were organized and aligned along myofibrils. However, in cardiomyocytes from Tg-miR-221 mice, the mitochondria were disorganized and dispersed, with degraded cristae (Figure 2a). In addition, a large amount of vacuoles with low electron densities were found in the cardiomyocytes from Tg-miR-221 mice (Figure 2a). These ultrastructural changes implied that the ability of the cell to clear damaged mitochondria might be impaired.

Given that autophagy is the primary process that mediates the bulk degradation of cytosolic proteins and organelles,[12] we speculated that this process might be impaired in miR-221 TG hearts. As expected, our results showed that the levels of the lipidated form of microtubule-associated protein 1 light chain 3 (LC3-II), a marker of autophagy, were dramatically decreased in Tg-miR-221 hearts (Figures 2b and c). Consistently, the levels of sequestosome 1 (p62), an indicator of cytosolic protein clearance, were significantly increased (Figures 2d and e). Thus, our data supported the hypothesis that autophagy was impaired in the hearts of Tg-miR-221 mice.

We further determined whether the inhibition of autophagy in Tg-miR-221 hearts was a direct effect of miR-221 overexpression. First, H9c2 cells were forced to overexpress miR-221 by the transient transfection of miR-221 mimics (Figure 2f). An autophagy-reporter plasmid encoding the EGFP-LC3 recombinant protein was also co-transfected into H9c2 cells, and the formation of autophagosomes was monitored based on the appearance of EGFP-LC3 puncta. H9c2 cells overexpressing miR-221 had significantly lower levels of punctate EGFP-LC3 compared with those of the control cells (Figures 2g and h). Consistently, LC3-II levels were also dramatically decreased in miR-221-overexpressing H9c2 cells (Supplementary Figure S2). Next, we tested the effect of miR-221 overexpression on autophagy in cultured neonatal rat cardiomyocytes by determining the levels of autophagy markers. Consistent with the findings in Tg-miR-221 heart tissues, cardiomyocytes transfected with miR-221 mimics had decreased levels of LC3-II and increased levels of p62 (Figures 2i–l). Conversely, knockdown of miR-221 with antagomir significantly increased the number of EGFP-LC3 puncta (Figures 3a and b) and levels of LC3-II (Figures 3c and d). These results indicate that miR-221 directly inhibit autophagy in cardiomyocytes.

To further determine the effect of miR-221 on autophagic flux, LC3 turnover assay was performed. H9c2 cells were transfected with miR-221 mimics or antagomir for 48 h, followed by incubating with lysosomal inhibitor chloroquine (CQ, 10 μm) for 1 h. As shown in Figures 3e–h, CQ could further increase the LC3-II levels both in miR-221-overexpressed or -silenced H9c2 cells compared with vehicle treatment. In the presence of CQ, miR-221 overexpression downregulated LC3-II level (Figures 3e and f). In contrast,

miR-221 silencing resulted in an increase of LC3-II level compared with control cells on CQ treatment (Figures 3g and h).

We next performed the mRFP-GFP-LC3 assay in H9c2 cells. As green fluorescent protein (GFP) fluorescence can be lysosomal quenched at acidic pH, red puncta accumulated when autophagic flux is stimulated, as treated with rapamycin. When autophagic flux was blocked in the autophagosome–lysosome fusion stage, as treated with Balfilomycin A1, only

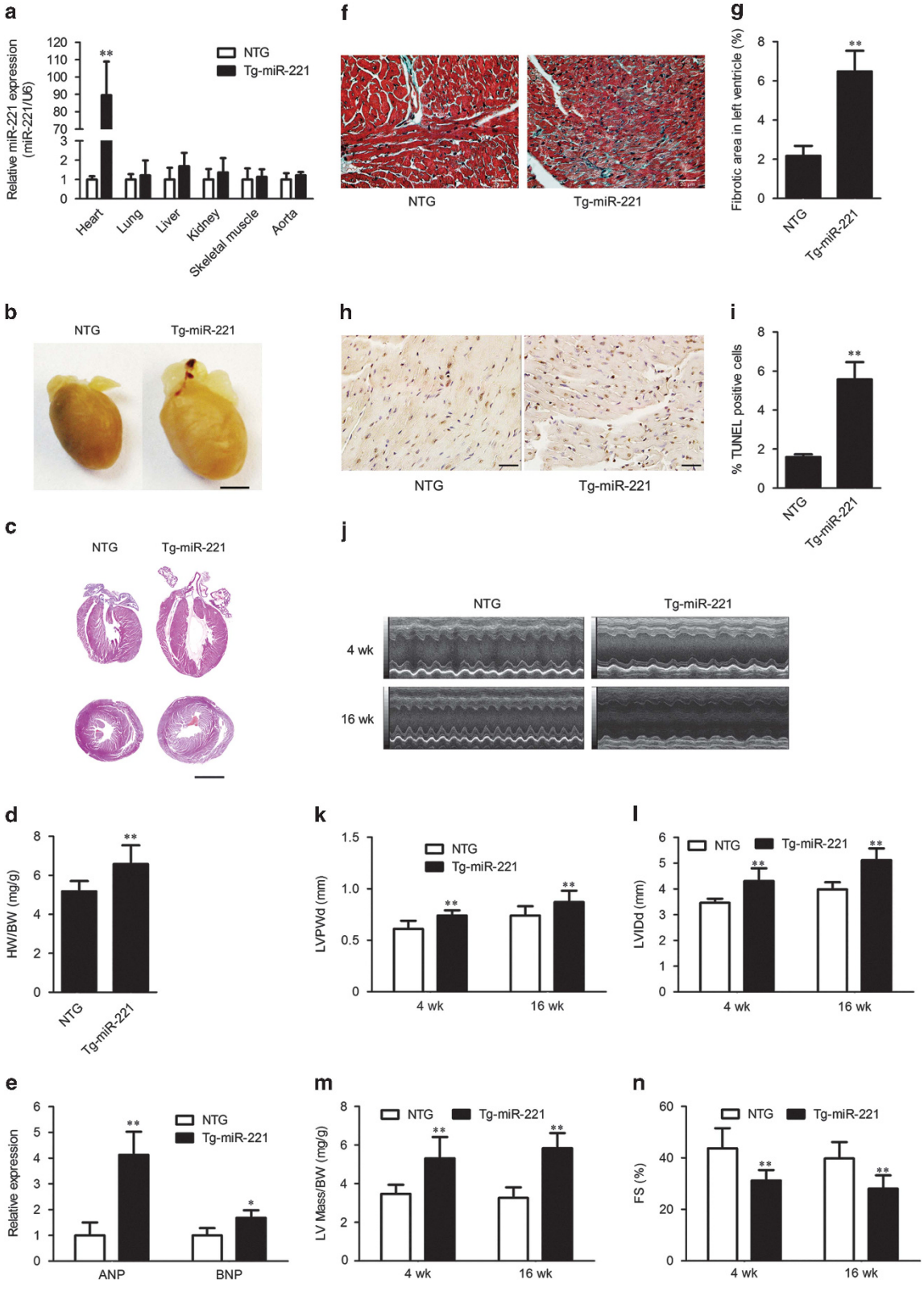

GFP^+/RFP^+ (merged as yellow) puncta accumulates. We observed that miR-221 overexpression resulted in a decrease of both yellow and red puncta, whereas knockdown of miR-221 induced an accumulation of both yellow and red puncta (Figures 3i and j). Taken together, these results indicated that miR-221 inhibited autophagic flux mainly through suppressing the formation rather than regulating the degradation of autophagic vesicles in cardiomyocytes.

Autophagy inhibition is indispensible for miR-221-induced pathological cardiac remodeling. As the mTOR is a well-known negative regulator of autophagy, we next examined whether it was involved in miR-221-induced autophagy inhibition. We first measured the activity of mTOR by detecting the phosphorylation levels of mTOR and its substrates (4E-BP1, S6K, or S6). At 4 weeks of age, phospho-mTOR (S2448), phospho-4E-BP1 (T37/46), and phospho-S6 (S235/236) levels were all significantly increased in TG hearts compared with those in the NTG controls (Figure 4a and Supplementary Figure S3A), indicating that mTOR was activated. Next, we assessed whether the activation of mTOR was a direct effect of miR-221 overexpression. In cultured neonatal rat cardiomyocytes, the transfection of miR-221 resulted in the hyperactivation of mTOR, as demonstrated by increased phospho-mTOR, phospho-S6K, and phospho-S6 (Figure 4b and Supplementary Figure S3*B*) levels. Conversely, miR-221 depletion decreased the levels of phospho-mTOR, phospho-S6K, and phospho-S6 (Figure 4c and Supplementary Figure S3*C*). These data suggested that miR-221 regulated the activity of mTOR in myocardiocytes.

Our previous study demonstrated that the overexpression of miR-221 induces cardiomyocyte hypertrophy *in vitro*. To assess whether the cardiac remodeling induced by miR-221 overexpression is dependent on the inhibition of autophagy, we inhibited the activity of mTOR and re-activated autophagy by either rapamycin treatment or knockdown of regulatory-associated protein of mTOR (Raptor) with two different siRNAs in cardiomyocytes. Raptor is an essential component of mTOR complex 1 (mTORC1).[17] Knockdown of Raptor caused impaired function of mTORC1 and increased autophagy.[18] In the present study, either knockdown of Raptor or rapamycin treatment significantly inhibited the miR-221-induced activation of mTOR, supported by the decreased levels of phosphorylated mTOR and its substrate, phospho-S6K, -4E-BP1, and S6 (Figures 4d and e, and Supplementary Figure S3D). Simultaneously, LC3-II levels were increased and p62 levels were decreased (Figures 4d and e,Supplementary Figure S3D). Furthermore, both raptor knockdown and rapamycin treatment attenuated the repression of EGFP-LC3 puncta formation induced by miR-221 in H9c2 cells (Figures 4f and g, and Supplementary Figure S3E and F), suggesting that the miR-221-induced inhibition of autophagy was dependent on mTOR activation. Consistent with our previous study, the overexpression of miR-221 increased the surface area of cultured neonatal rat cardiomyocytes (Figures 4h and I, and Supplementary Figure S3G and H). Knockdown of Raptor or rapamycin treatment significantly antagonized the hypertrophic effect of miR-221 overexpression (Figures 4h and I, and Supplementary Figure S3G and H). The expression levels of both ANP and BNP in miR-221-overexpressing cardiomyocytes were also restored to levels similar to those observed in the control cells (Supplementary Figure S3I–L). Thus, re-activation of autophagy rescued miR-221-induced cardiomyocyte hypertrophy *in vitro*. Taken together, our results indicated that the inhibition of autophagy induced by miR-221 overexpression was dependent on mTOR activation and was necessary for miR-221-induced pathogenic cardiac remodeling.

MiR-221 activates mTOR in a p27/CDK2-dependent manner. Previously, we determined that p27 was a direct target of miR-221 in cardiomyocytes *in vitro*.[9] Consistently, in the present study, we observed that the *in vivo* expression levels of p27 were significantly downregulated by the TG overexpression of miR-221 in mouse hearts (Figures 5a and b). To determine whether the suppression of p27 was responsible for the inhibition of autophagy induced by miR-221 overexpression, we knocked down p27 using two different siRNAs in H9c2 cells. As shown in Figure 5c, the expression levels of p27 were markedly repressed by both siRNAs. P27 knockdown significantly reduced the lipidation levels of LC3 protein and increased the levels of p62 (Figures 5d and e), indicating that the downregulation of p27 alone was sufficient to inhibit autophagy. As expected, the mTOR pathway was also markedly activated in H9c2 cells in which the expression of p27 was suppressed, as demonstrated by the increased phosphorylation levels of both mTOR and S6K (Figures 5d and e).

We next restored the expression of p27 in H9c2 cells with miR-221 overexpression. Forced expression of p27 reversed the level of LC3-II and decreased the accumulation of p62 and the phosphorylation level of S6K (Figures 5f and g). Consistently, the inhibited formation of EGFP-LC3 puncta by miR-221 was also restored to normal level (Figures 5h and i). Thus, our results demonstrated that upregulating p27 rescued miR-221-induced mTOR activation and autophagy inhibition.

To determine whether p27 overexpression induced autophagy activation or impaired degradation of autophagic

Figure 1 Cardiac-specific overexpression of miR-221 in mice induces heart failure. (**a**) Expression levels of miR-221 in the indicated tissues of NTG and miR-221 TG (Tg-miR-221) mice, as assayed by quantitative real-time PCR analysis. U6 was used as an internal control ($n=8$ per group). (**b**) The morphology of explanted hearts from NTG and Tg-miR-221 mice at 4 weeks of age. Scale bar: 2 mm. (**c**) Hematoxylin and eosin staining of sections (upper panel, sagittal; lower panel, transverse) from NTG and Tg-miR-221 hearts. Scale bars: 2 mm. (**d**) Ratios of heart weight to body weight (HW/BW) of NTG and Tg-miR-221 mice at 4 weeks of age ($n=8$ per group). (**e**) Expression levels of ANP and BNP in hearts from NTG and Tg-miR-221 mice, quantified by real-time PCR ($n=6$ per group). GAPDH was used as a housekeeping control gene. (**f**) Masson's trichrome-stained myocardia from NTG and Tg-miR-221 mice. Scale bars: 20 μm. (**g**) Morphometric analysis of cardiac fibrosis from NTG and Tg-miR-221 hearts ($n=4$ per group). (**h**) TUNEL labeling of nuclei in myocardia from NTG and Tg-miR-221 mice. Scale bars, 20 μm. (**i**) The percentages of TUNEL-positive cells in myocardia from NTG and Tg-miR-221 mice ($n=4$ per group). (**j**) Representative M-mode images of transthoracic echocardiography. Quantification of the left ventricular posterior wall thickness at the end of diastole (LVPWd; **k**), internal dimension of the left ventricle at the end of diastole (LVIDd; **l**), left ventricular mass/body weight ratio (LV Mass/BW; **m**), and fractional shortening (FS %; **n**) of hearts from NTG and Tg-miR-221 mice at 4 and 16 weeks of age; $n=8$ per group. The data are expressed as the mean $\pm$ S.D.; $^*P<0.05$ and $^{**}P<0.01$ compared with the NTG group

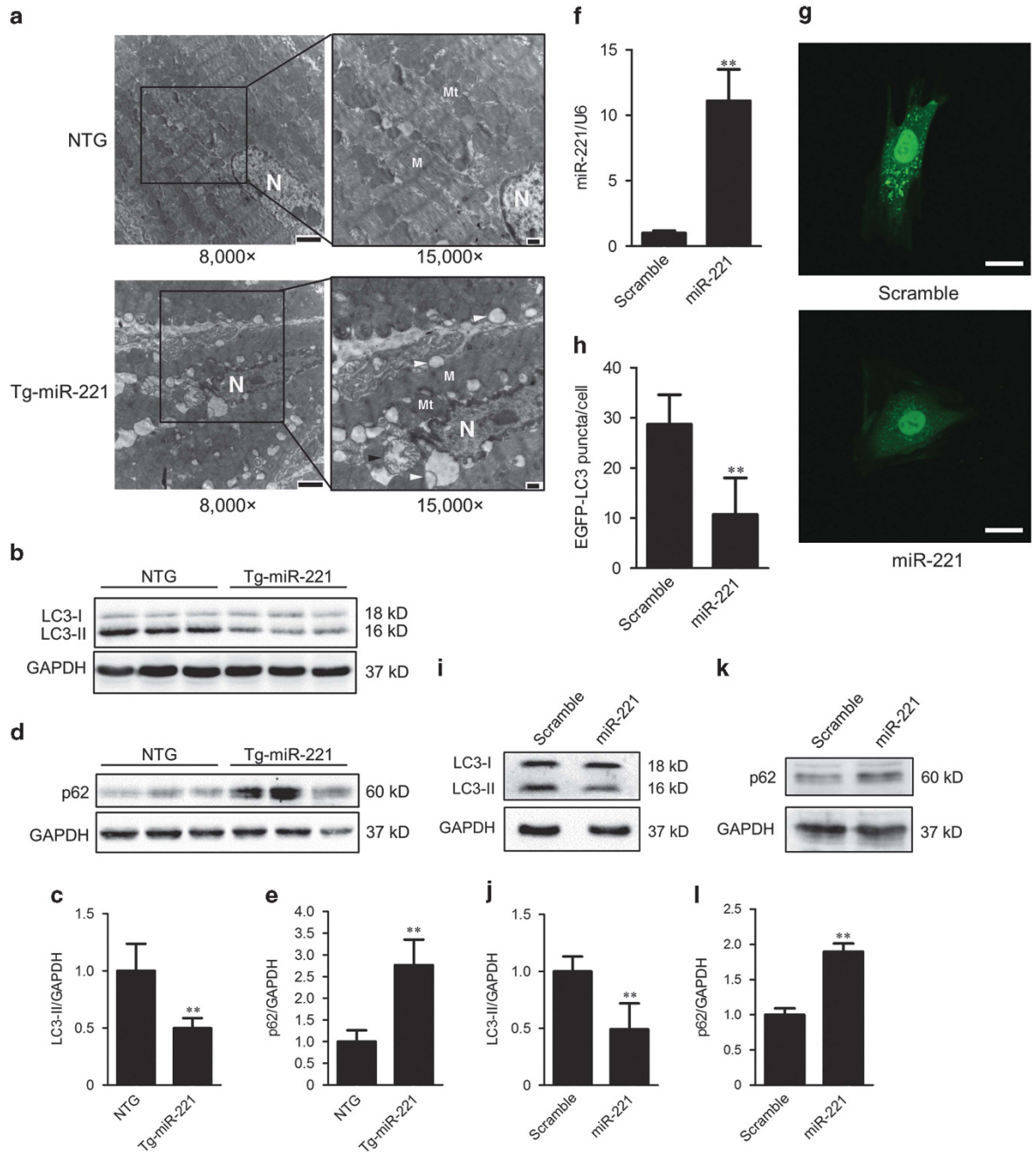

Figure 2 MiR-221 inhibits autophagy *in vivo* and *in vitro*. (**a**) The myocardial ultrastructure of NTG ($n=4$) and miR-221 TG (Tg-miR-221, $n=6$) mice were stained with uranyl acetate and analyzed by transmission electron microscopy. Representative graphs are shown (N: nucleus, M: muscle fibers, Mt: mitochondria, black arrow head: damaged mitochondria, white arrow head: low electron density vacuoles. Scale bars: left panel, 2 μM; right panel, 0.5 μm). Western blot analysis of the levels of LC3 (**b** and **c**) and sequestosome 1 (p62; **d** and **e**) in hearts from NTG and Tg-miR-221 mice ($n=6$). (**f**) Expression levels of miR-221 in H9c2 cells transfected with scramble or miR-221 mimics, assayed by quantitative real-time PCR analysis. U6 was used as an internal control ($n=3$ per group). Representative images (**g**) and quantification (**h**) of EGFP-LC3 puncta (green) in H9c2 cells transfected with miR-221 mimics or scrambled control together with pEGFP-LC3 plasmid. Scale bars: 20 μM. Neonatal rat cardiomyocytes were transfected with miR-221 mimics or scrambled control, after which the lipidation levels of LC3 (**i** and **j**) and the expression levels of p62 (**k** and **l**) were determined by using western blotting. The data were obtained from at least three independent experiments and the values represent the means ± S.D. $^{**}P<0.01$ compared with NTG control mice or scrambled control

vesicles, autophagic flux was analyzed. As is shown in Figures 5j and k, lysosomal inhibitor CQ could further increase LC3-II level in H9c2 cells with miR-221 and p27 overexpression. The results from mRFP-GFP-LC3 assay also showed that p27 overexpression induced the accumulation of both the yellow and red puncta (Supplementary Figure S4). Taken together, these results demonstrated that p27 mediated the regulation of miR-221 on mTOR and autophagy in cardiomyocytes.

To elucidate the molecular mechanism by which p27 mediates miR-221-induced mTOR activation and autophagy inhibition, we first determined the activity levels of AKT, ERK1/2, and AMPKα, which are representatives of three

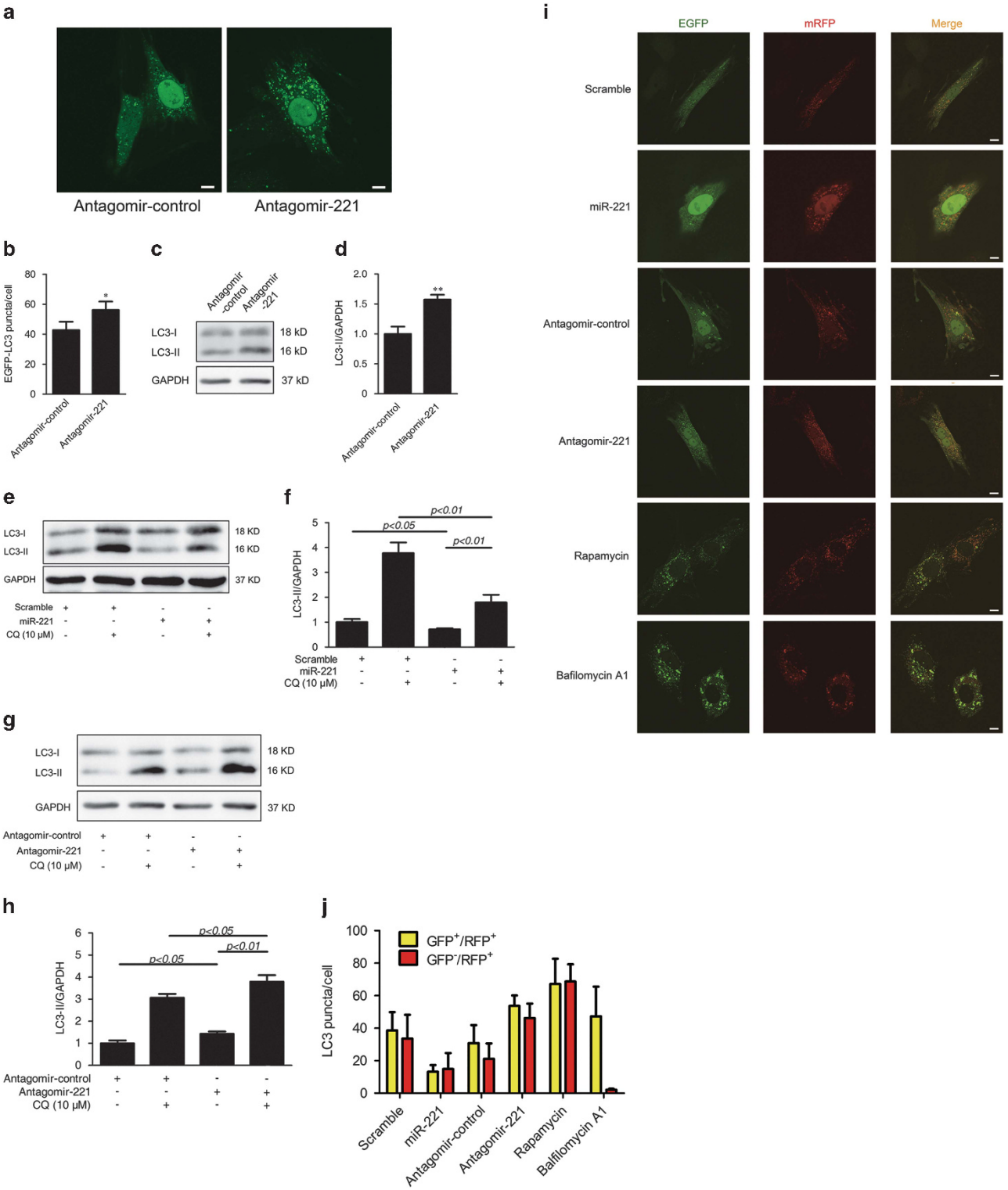

Figure 3 Knockdown of miR-221 stimulates autophagic flux. Representative images (**a**) and quantification (**b**) of EGFP-LC3 puncta (green) in H9c2 cells transfected with miR-221 antagomir or control together with pEGFP-LC3 plasmid. Scale bars: 10 μM. (**c** and **d**) Lipidation levels of LC3 in H9c2 cells were transfected with miR-221 antagomir or control antagomir. H9c2 cells were transfected with scramble or miR-221 mimics (**e** and **f**) and miR-221 or control antagomir (**g** and **h**) in the presence or absence of 10 μM chloroquine (CQ) as indicated. Western blotting was performed to detect the LC3 levels. (**i** and **j**) H9c2 cells transiently expressing mRFP-GFP-LC3 were co-transfected with scramble or miR-221 mimics, control or miR-221 antagomir for 48 h, or treated with rapamycin (200 nM) or Balfilomycin A1 (100 nM) for 2 h, as indicated. The cells were visualized by confocal microscopy (**i**). Scale bars: 10 μM. The number of GFP^+/RFP^+ (yellow) and GFP^-/RFP^+ (red) dots per cell were quantified (**j**). The data were obtained from at least three independent experiments, and the values represent the means ± S.D. $^*P<0.05$ and $^{**}P<0.01$ compared with antagomir control

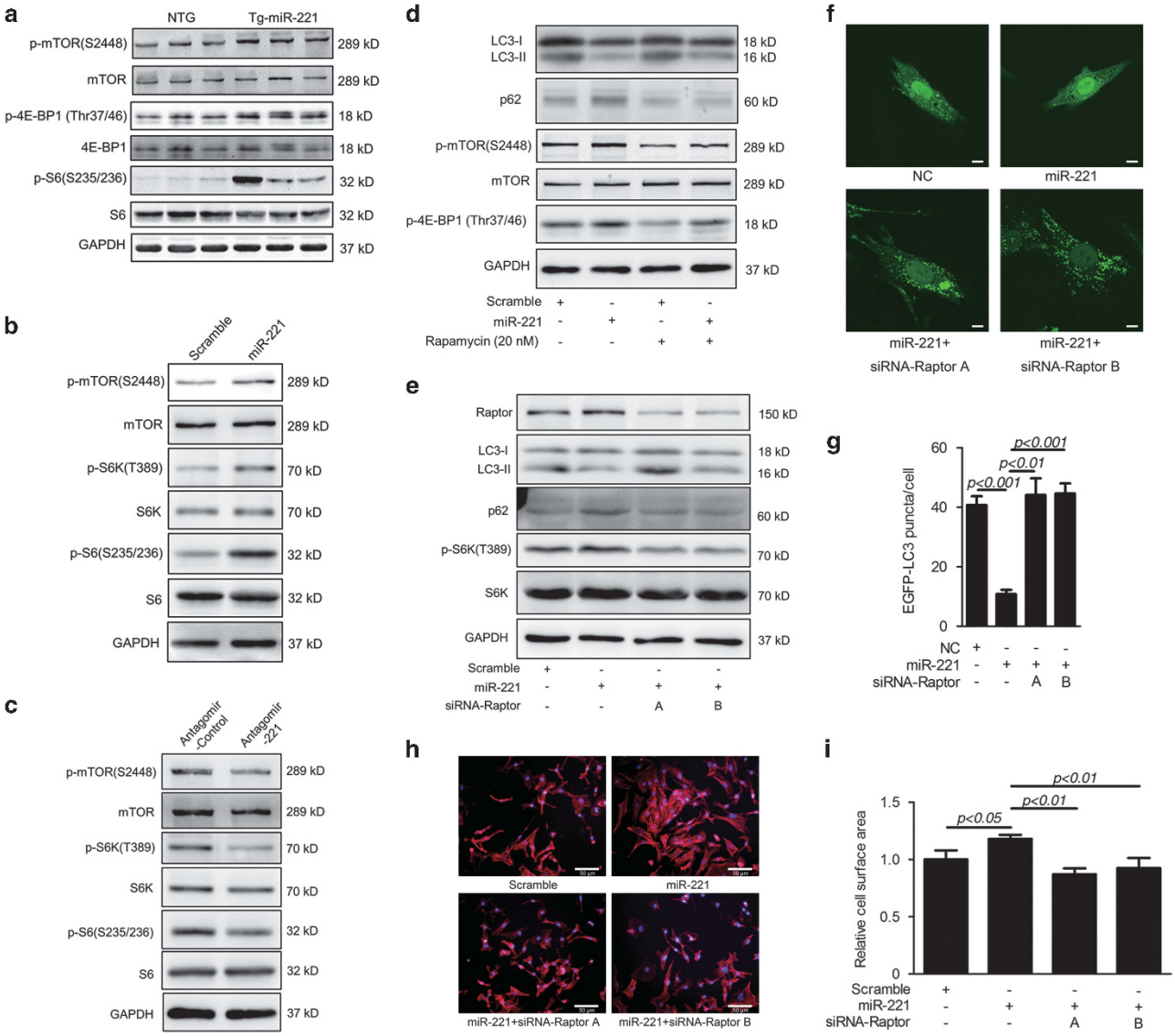

Figure 4 Overexpression of miR-221 activates the mTOR signaling pathway. (**a**) Western blot analysis of phosphorylated mTOR (p-mTOR), 4E-BP1 (p-4E-BP1), and S6 (p-S6) in hearts from non-transgenic (NTG) and miR-221 transgenic (Tg-miR-221) mice. ($n=6$ per group). (**b**) The phosphorylation status of mTOR, S6K (p-S6K), and S6 in neonatal rat cardiomyocytes transfected with miR-221 mimics or scrambled control. (**c**) The phosphorylation of mTOR, S6K (p-S6K), and S6 in H9c2 cells transfected with miR-221 antagomir or control. Rapamycin (**d**) or knockdown of Raptor (**e**) abolishes miR-221-induced mTOR activation and autophagy inhibition. Cardiomyocytes were transfected with miR-221 mimics or scrambled control and treated with rapamycin (20 nM; **d**) or co-transfected with two specific siRNAs targeting Raptor (**e**). The phosphorylation levels of mTOR, S6K, 4E-BP1, the lipidation levels of LC3, and the expression levels of p62 were measured by western blottings. (**f** and **g**) Knockdown of Raptor attenuates the miR-221-induced repression of autophagosome formation. H9c2 cells transiently expressing pEGFP-LC3 fusion protein were co-transfected with miR-221 mimics or scrambled control and Raptor-specific siRNAs, as indicated. EGFP-LC3 puncta (green) were observed by confocal microscopy. Scale bars, 10 μM. (**h** and **i**) Raptor knockdown rescues the cardiomyocyte hypertrophy induced by miR-221 overexpression. Cultured neonatal rat cardiomyocytes were transfected and treated, as indicated. F-actin and the nuclei of cultured neonatal rat cardiomyocytes were stained with Texas Red-phalloidin and DAPI, respectively. Scale bars: 50 μm (**h**). The cell surface area was quantified with Image Pro-Plus 6.0 (**i**)

Figure 5 MiR-221 regulates mTOR and autophagy by suppressing p27 expression. (**a** and **b**) Expression levels of p27 in the hearts of non-transgenic (NTG) and miR-221 transgenic (Tg-miR-221) mice ($n=6$ per group). Representative images (**a**) and relative expression intensities (**b**) of p27 are shown. H9c2 cells were transfected with negative control (NC) or two different siRNAs to knock down p27 (**c**). The lipidation levels of LC3, expression levels of p62, and phosphorylation status of mTOR and S6K were measured (**d**) and quantified (**e**). $^{*}P<0.05$, $^{**}P<0.01$ compared with the NC group. (**f** and **g**) P27 was forced to express in H9c2 cells transfected with miR-221 or scramble control. The phosphorylation status of S6K, levels of LC3-II and p62 are shown (**f**) and quantified (**g**). $^{*}P<0.05$ and $^{**}P<0.01$ compared with scramble+pcDNA3.1 group, and $^{\#}P<0.05$ and $^{\#\#}P<0.01$ compared with the miR-221+pcDNA3.1 group. Representative images (**h**) and quantification (**i**) of EGFP-LC3 puncta (green) in H9c2 cells transfected as indicated. Scale bars: 10 μM. (**j** and **k**) H9c2 cells were transfected as indicated and incubated in the presence or absence of 10 μM chloroquine (CQ). Western blotting was performed to detect the LC3 levels. The data were obtained from at least three independent experiments, and the values are expressed as the means $\pm$ S.D.

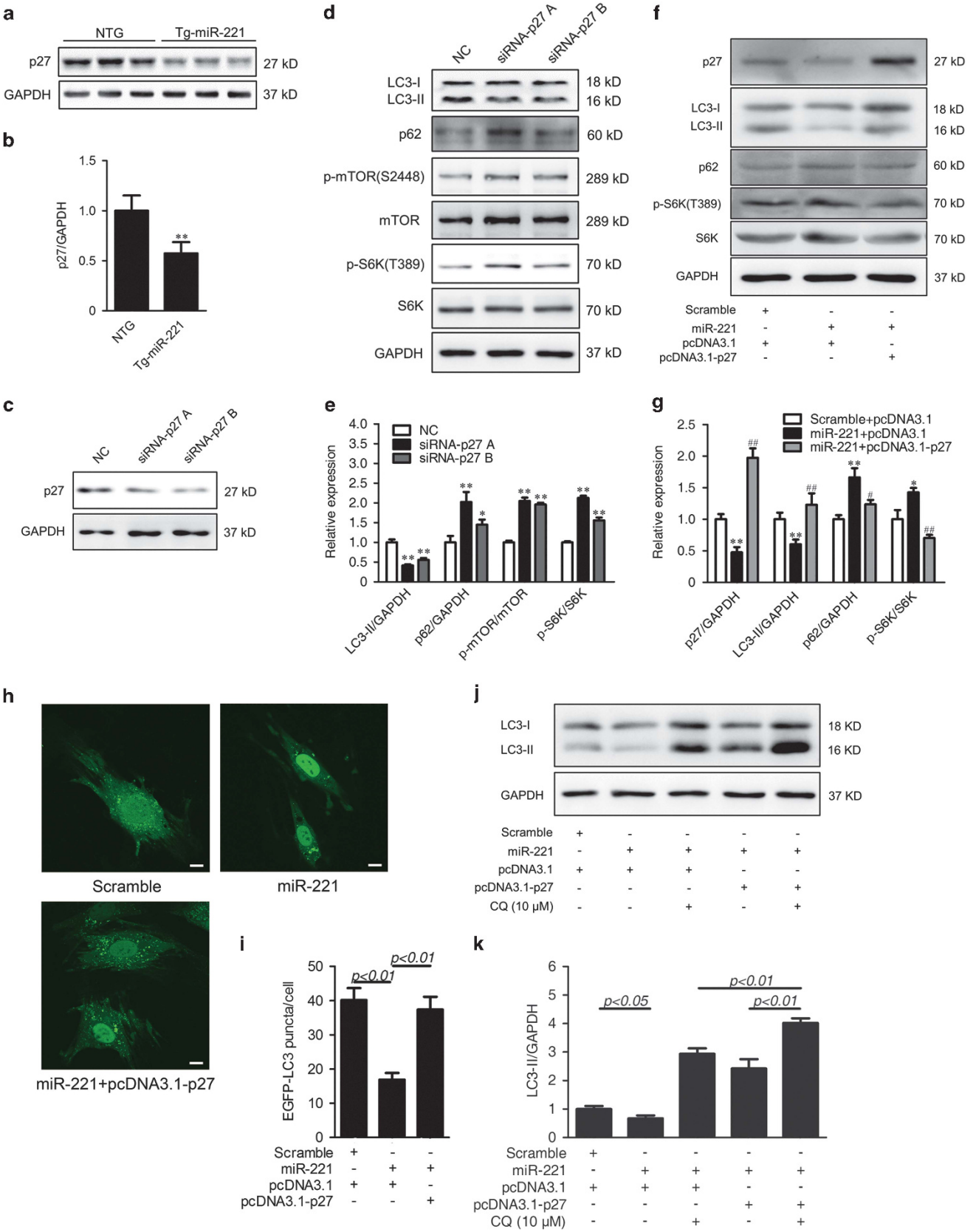
a
NTG
Tg-miR-221
p27
27 kD
GAPDH
37 kD
b
p27/GAPDH
1.5
1.0
0.5
0
**
NTG
Tg-miR-221
c
NC
siRNA-p27 A
siRNA-p27 B
p27
27 kD
GAPDH
37 kD
d
NC
siRNA-p27 A
siRNA-p27 B
LC3-I
LC3-II
18 kD
16 kD
p62
60 kD
p-mTOR(S2448)
289 kD
mTOR
289 kD
p-S6K(T389)
70 kD
S6K
70 kD
GAPDH
37 kD
e
Relative expression
NC
siRNA-p27 A
siRNA-p27 B
LC3-II/GAPDH
p62/GAPDH
p-mTOR/mTOR
p-S6K/S6K
f
p27
27 kD
LC3-I
LC3-II
18 kD
16 kD
p62
60 kD
p-S6K(T389)
70 kD
S6K
70 kD
GAPDH
37 kD
Scramble + - -
miR-221 - + +
pcDNA3.1 + + -
pcDNA3.1-p27 - - +
g
Relative expression
Scramble+pcDNA3.1
miR-221+pcDNA3.1
miR-221+pcDNA3.1-p27
p27/GAPDH
LC3-II/GAPDH
p62/GAPDH
p-S6K/S6K
h
Scramble
miR-221
miR-221+pcDNA3.1-p27
i
EGFP-LC3 puncta/cell
p<0.01
p<0.01
Scramble + - -
miR-221 - + +
pcDNA3.1 + + -
pcDNA3.1-p27 - - +
j
LC3-I
LC3-II
18 KD
16 KD
GAPDH
37 KD
Scramble + - - - -
miR-221 - + + + +
pcDNA3.1 + + + - -
pcDNA3.1-p27 - - - + +
CQ (10 μM) - - + - +
k
LC3-II/GAPDH
p<0.05
p<0.01
p<0.01
Scramble + - - - -
miR-221 - + + + +
pcDNA3.1 + + + - -
pcDNA3.1-p27 - - - + +
CQ (10 μM) - - + - +

well-known upstream signaling pathways of mTOR. AKT and ERK1/2 are positive regulators of mTOR, whereas AMPK*α* is a negative regulator of mTOR.[19–22] We found that the phosphorylation levels of AMPK*α* (T172) and ERK1/2 (T202/Y204) were comparable between Tg-miR-221 and NTG mice, as well as between miR-221-overexpressing and control cultured neonatal rat cardiomyocytes. The phosphorylation levels of AKT at both the S473 and T308 sites were much higher in the heart tissues of Tg-miR-221 mice compared with those of NTG mice (Figures 6a and b). However, the overexpression of miR-221 did not alter the phosphorylation levels of AKT *in vitro* (Figures 6c and d), suggesting that the activation of AKT in the hearts of Tg-miR-221 mice was most likely due to the development of heart failure rather than being a direct effect of miR-221 overexpression. Collectively, these results demonstrated that the classical AKT, ERK1/2, and AMPK*α* signaling pathways were not directly involved in the mTOR activation and autophagy inhibition induced by miR-221 overexpression.

P27 has been regarded as a pro-autophagic protein by downregulation of Bcl-2, an autophagy inhibitor, via the Rb/E2F1 axis.[23,24] We next examined whether the overexpression of miR-221 could upregulate Bcl-2, because it significantly suppressed the expression of p27. Contrary to expectations, Bcl-2 protein levels were reduced in the hearts of Tg-miR-221 mice compared with those of NTG mice (Figures 6e and f). Moreover, the *in vitro* overexpression of miR-221 did not alter the expression of Bcl-2 in cardiomyocytes (Figures 6g and h). Therefore, our data suggested that Bcl-2 was not involved in the p27-mediated autophagy inhibition induced by miR-221 overexpression in cardiomyocytes.

P27 is also known as a CDK inhibitor that interacts with CDK2 to inhibit the cell cycle.[25,26] In cardiomyocytes, the robust expression of p27 leads to CDK2 inhibition, maintaining cell cycle quiescence.[27] Next, we investigated whether miR-221-induced autophagy inhibition and mTOR activation were dependent on CDK2 activity. We employed SU9516, a selective CDK2 inhibitor, to suppress CDK2 activity. In neonatal rat cardiomyocytes overexpressing miR-221, SU9516 treatment significantly reduced the phosphorylation levels of S6K and S6, indicating that the activation of mTOR was repressed (Figure 6i). Consistently, the lipidation levels of LC3 and p62 were upregulated and downregulated, respectively, by SU9516 (Figure 6j). In miR-221-overexpressing H9c2 cells, SU9516 treatment restored the number of EGFP-LC3 puncta to normal levels (Figures 6k and l), suggesting that the inhibition of CDK2 rescued the impaired autophagy induced by miR-221 overexpression. Similarly, SU9516 also attenuated the hyperactivation of mTOR and decreased the lipidation levels of LC3 induced by p27 knockdown in cardiomyocytes (Figure 6m). Furthermore, SU9516 completely antagonized the cardiac hypertrophy induced by miR-221 overexpression in cultured neonatal rat cardiomyocytes, indicating that miR-221-induced cardiac hypertrophy was CDK2 dependent (Figures 6n and o).

We further suppressed the expression of CDK2 with two different siRNAs (Figure 7a). Similarly, knockdown of CDK2 inhibited the activity of mTOR and increased autophagy in miR-221-overexpressed cardiomyocytes (Figures 7a and b), and restored the inhibited formation of EGFP-LC3 puncta in H9c2 cells (Figures 7c and d). To analyze whether CDK2 inhibition could stimulate autophagic flux, we treated cells in the presence or absence of CQ. As shown in Figures 7e and f, CQ could further increase the LC3-II levels of CDK2-depleted H9c2 cells with miR-221 overexpression. Consistently, the mRFP-GFP-LC3 confocal microscopy assay showed accumulation of both yellow and red puncta in miR-221-overexpressed H9c2 cells on CDK2 silencing (Supplementary Figure S5). Similar to SU9516 treatment, CDK2 knockdown also rescued the cardiomyocyte hypertrophy induced by miR-221 overexpression (Figures 7g and h). Thus, our results indicated that CDK2 acted as a downstream mediator of p27 and was required for the autophagy inhibition and pathological cardiac remodeling induced by miR-221 overexpression in cardiomyocytes (Figure 8).

Discussion

MiRNAs are essential to the regulation of cardiac remodeling;[3–8] however, many of them have not been well characterized. We previously demonstrated that miR-221 induces cardiomyocyte hypertrophy *in vitro*.[9] In the present study, we demonstrated that the cardiac-specific TG overexpression of miR-221 in mice resulted in cardiac dysfunction and heart failure *in vivo*, as evidenced by severe cardiac enlargement, increased interstitial fibrosis, and impaired cardiac function. Our present study confirmed and extended our previous discoveries, revealing that miR-221 is an important regulator of cardiac homeostasis and remodeling and therefore might be a potential therapeutic target for heart failure.

Proper autophagy level is required to maintain cardiac homeostasis and function. Disrupted autophagy has been demonstrated to contribute to cardiac remodeling.[13,28,29] mTOR is a pivotal upstream mediator of autophagy through its binding and inactivation of the autophagy kinase complex ULK1/2, thereby blocking the formation of autophagosomes.[30]

Figure 6 CDK2 is required for miR-221-induced autophagy inhibition and cardiac remodeling. Phosphorylated AKT (p-AKT), ERK (p-ERK), and AMPKα (p-AMPKα) in myocardia from non-transgenic (NTG) and miR-221 transgenic (Tg-miR-221) mice ($n=6$ per group; **a** and **b**), and cultured neonatal rat cardiomyocytes transfected with miR-221 mimics or scrambled control (**c** and **d**). Expression of Bcl-2 in myocardia from wild-type and Tg-miR-221 mice ($n=6$ per group; **e** and **f**) and cultured neonatal rat cardiomyocytes transfected with scrambled control or miR-221 mimics (**g** and **h**). Cultured neonatal rat cardiomyocytes were transfected with miR-221 mimics or scrambled control and treated with SU9516, a selective inhibitor of CDK2, as indicated. The phosphorylation status of S6K (p-S6K) and S6 (p-S6) (**i**), the lipidation level of LC3, and the expression level of p62 (**j**) were determined by western blottings. H9c2 cells were co-transfected with pEGFP-LC3 plasmid and miR-221 mimics or scrambled control, and treated with SU9516 (5 μM), as indicated. EGFP-LC3 puncta (green) were observed by confocal microscopy (**k**) and quantified (**l**). Scale bars: 20 μM. (**m**) Neonatal rat cardiomyocytes were transfected with two different siRNAs for knockdown of p27 and treated with SU9516 (5 μM). The lipidation levels of LC3 and the phosphorylation status of S6K (p-S6K) were measured with western blottings. (**n** and **o**) Neonatal rat cardiomyocytes were transfected and treated with SU9516 (5 μM), as indicated. F-actin and nuclei were stained with Texas Red-phalloidin and DAPI, respectively. Scale bars: 50 μM (**n**). The cell surface area was quantified with Image Pro-Plus 6.0 (**o**). The data were obtained from at least three independent experiments, and the values represent the means $\pm$ S.D. $^*P<0.05$, $^{**}P<0.01$ compared with the NTG group

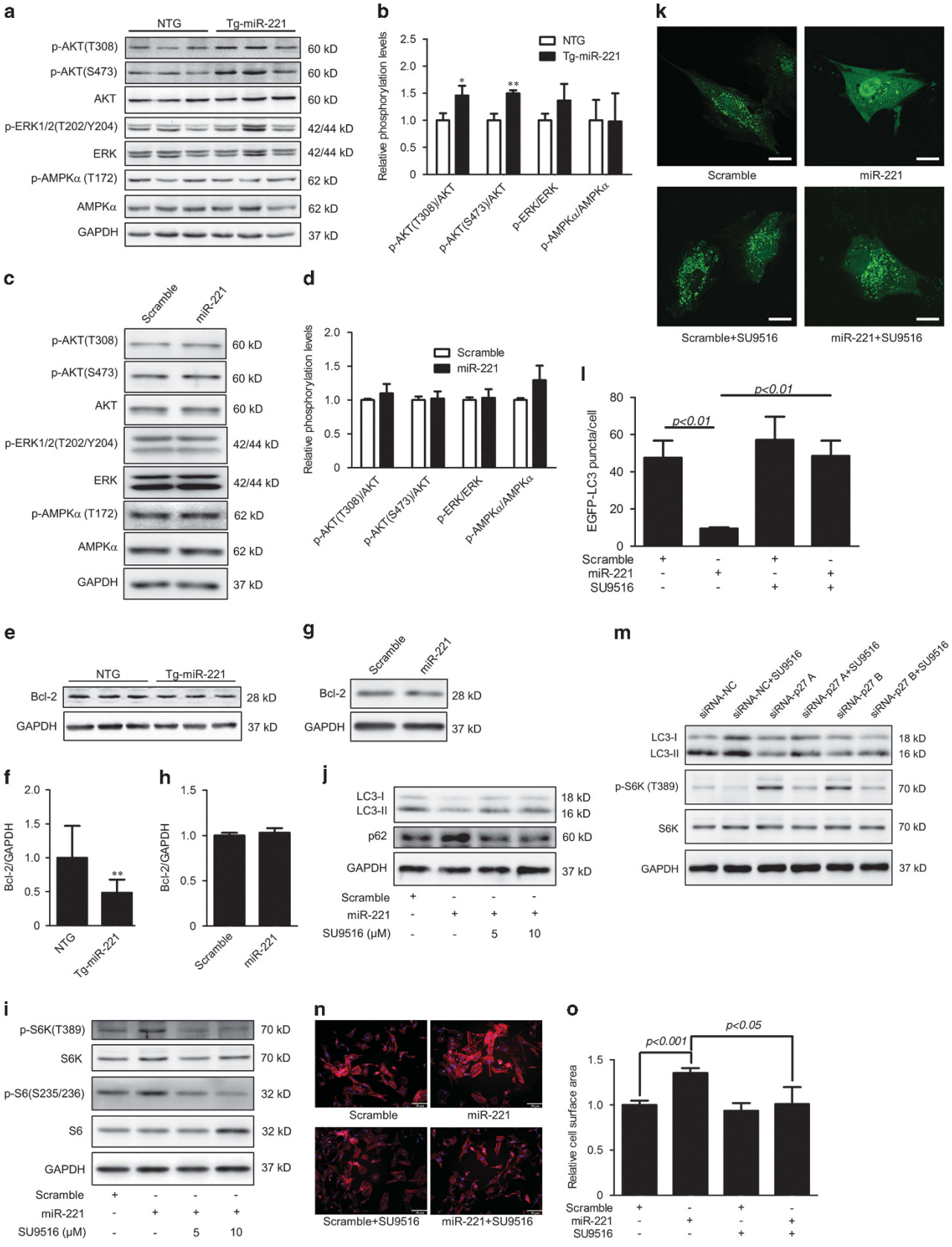
a
NTG
Tg-miR-221
p-AKT(T308)
p-AKT(S473)
AKT
p-ERK1/2(T202/Y204)
ERK
p-AMPKα (T172)
AMPKα
GAPDH
60 kD
60 kD
60 kD
42/44 kD
42/44 kD
62 kD
62 kD
37 kD
b
Relative phosphorylation levels
NTG
Tg-miR-221
p-AKT(T308)/AKT
p-AKT(S473)/AKT
p-ERK/ERK
p-AMPKα/AMPKα
k
Scramble
miR-221
Scramble+SU9516
miR-221+SU9516
c
Scramble
miR-221
d
Relative phosphorylation levels
Scramble
miR-221
l
EGFP-LC3 puncta/cell
p<0.01
p<0.01
Scramble
miR-221
SU9516
e
NTG
Tg-miR-221
Bcl-2
GAPDH
28 kD
37 kD
g
Scramble
miR-221
m
siRNA-NC
siRNA-NC+SU9516
siRNA-p27 A
siRNA-p27 A+SU9516
siRNA-p27 B
siRNA-p27 B+SU9516
LC3-I
LC3-II
p-S6K (T389)
S6K
GAPDH
18 kD
16 kD
70 kD
70 kD
37 kD
f
Bcl-2/GAPDH
NTG
Tg-miR-221
h
Bcl-2/GAPDH
Scramble
miR-221
j
LC3-I
LC3-II
p62
GAPDH
18 kD
16 kD
60 kD
37 kD
Scramble
miR-221
SU9516 (μM)
i
p-S6K(T389)
S6K
p-S6(S235/236)
S6
GAPDH
70 kD
70 kD
32 kD
32 kD
37 kD
Scramble
miR-221
SU9516 (μM)
n
Scramble
miR-221
Scramble+SU9516
miR-221+SU9516
o
Relative cell surface area
p<0.001
p<0.05
Scramble
miR-221
SU9516

mTOR has also been found to have an important role in the maintenance of cardiac function. The cardiomyocyte-specific deletion of mTOR results in severe dilated cardiomyopathy,[31] whereas the pharmacological inhibition of mTOR reverses cardiac hypertrophy.[32–34] In the present study, we found that the overexpression of miR-221 impaired autophagy in cardiomyocytes both *in vivo* and in *vitro*; this was accompanied by mTOR activation. Conversely, blocking mTOR activation and re-activating autophagy with rapamycin treatments completely rescued miR-221-induced cardiomyocyte remodeling. Thus, our present study demonstrated that miR-221 promotes heart failure by regulating mTOR activity and autophagy, and provided further evidence that the appropriate level of autophagy is essential for the maintenance of cardiac function.

Several signaling pathways have been characterized to regulate autophagy in response to stress and starvation. AKT and ERK activate mTOR to inhibit autophagy,[29,35,36] whereas AMPK inhibits the activity of mTOR and thereby promotes autophagy.[37,38] On the other hand, there are studies indicating that AKT may also be activated by mTOR.[39] However, in the present study we found that ERK and AMPK were not affected both *in vivo* and *in vitro* by miR-221 overexpression. AKT was activated in the hearts of Tg-miR-221 mice, but its phosphorylation was not altered in cultured cardiomyocytes. Thus, our results indicate that these pathways were not involved in the miR-221-dependent regulation of autophagy and cardiac remodeling. The hyperphosphorylation of AKT may be a compensative response to cardiac remodeling rather than a direct downstream effect of either miR-221 overexpression or mTOR activation.

Instead, we found that miR-221 inhibited autophagy through the targeted repression of p27, thereby releasing the p27-mediated inhibition of CDK2 and subsequently activating mTOR. P27 is a well-known CDK inhibitor that can physically interact with and block the activity of CDKs.[27] Thereby, it inhibits cell cycle and induces apoptosis. In cardiomyocytes, p27 was also found to act as an anti-hypertrophic factor and is downregulated during heart failure and cardiac hypertrophy induced by pressure overload.[40,41] We previously found that p27 is a direct target of miR-221 in cardiomyocytes.[9] In the present study, the TG overexpression of miR-221 significantly suppressed the expression of p27 in mouse hearts. Knockdown of p27 alone was able to mimic the effects of miR-221 overexpression in cardiomyocytes, including mTOR activation and autophagy impairment. Furthermore, the inhibition of CDK2 attenuated the activation of mTOR, reversed the autophagy impairment, and rescued the cardiomyocyte hypertrophy induced by either miR-221 overexpression or p27 knockdown. Collectively, our findings demonstrated that miR-221 regulates autophagy and promotes heart failure by modulating the p27/CDK2/mTOR axis (Figure 8).

Interestingly, p27 was previously hypothesized to promote autophagy in cancer cells by downregulating the expression of the anti-autophagic inhibitor Bcl-2, functioning independently from mTOR.[24] However, although p27 levels were significantly suppressed, we did not find any increase in the expression levels of Bcl-2 in cardiomyocytes overexpressing miR-221, either *in vitro* or *in vivo*. In contrast, we found that mTOR activity was tightly regulated by p27/CDK2 and was indispensable for p27-mediated autophagy inhibition induced by miR-221. Thus, unlike what was reported in cancer cells, our results indicated that p27 regulates autophagy in cardiomyocytes through a novel pathway.

In a previous study, we found that miR-221 was moderately increased in the heart of patients with HCM, who usually suffer a slower cardiac remodeling process than that demonstrated in the TG mice with robust overexpression of miR-221.[9] Furthermore, p27, the direct target of miR-221, was decreased in pressure-overload hypertrophy and human heart failure.[40,41] P27 knockout mice developed cardiac hypertrophy and heart failure.[42] Most recently, Sun *et al.*[43] reported that p27 can protect cardiomyocyte from glucose-induced apoptosis by promoting autophagy. Thus, the miR-221 signal pathway might contribute to the cardiac remodeling in various human cardiovascular diseases, and which needs to be verified by more studies.

In conclusion, we found that miR-221 promoted cardiac remodeling through mTOR-mediated autophagy inhibition. A previously unknown signaling pathway, the p27/CDK2/mTOR, governed the regulation of autophagy by miR-221 in cardiomyocytes. Our study provides insights into the regulation of cardiomyocyte autophagy by miRNAs and implicates miR-221 as a potential therapeutic target for heart failure.

Materials and Methods

Animal studies. All animal studies were performed in accordance with the relevant guidelines and regulations,[44] and were approved by the Ethics Committee for Animal Study of Fuwai Hospital. A 533-bp fragment of mouse genomic DNA encoding the miR-221 precursor was amplified by PCR, using the primers 5′-GCTG TCGACGTCTTCCTCTTTCCCCCAT-3′ and 5′-CGAAGCTTGTGAGACCATTATTT GCTATGATG-3′. The amplified fragment was then cloned into the *Sal*I/*Hind*III sites downstream of the murine cardiac α-MHC promoter. After linearization with *Not*I, the transgene was injected into the pronucleus of fertilized zygotes from C57BL/6J, which were then transferred to the oviducts of pseudopregnant ICR recipients. The TG founders and their progeny were identified by the PCR analyses with tail genomic DNA, using the primers 5′-TTGCCTTGCCTTCTTGCG-3′ and 5′-ATTCG ATTGGTGGTCATTCATCATGCTATT-3′. The *Fabpi* gene was amplified as an internal control for PCR quality, using the primers 5′-TGGACAGGACTGGACC TCTGCTTTCCTAGA-3′ and 5′-TAGAGCTTTGCCACATCACAGGTCATTCAG-3′. Male TG mice at 4 and 16 weeks of age were used for functional and histological studies, and were compared with their NTG littermates.

Transthoracic echocardiography. Transthoracic echocardiography was performed as described previously.[45] Briefly, mice were weighed and anesthetized with 2.5% avertin (0.018 ml/g), given i.p., and the two-dimensional short and long axes of the left ventricle (LV) were viewed by using a 30-MHz probe interfaced with a Vevo-770 high-frequency ultrasound system (VisualSonics, Toronto, ON, Canada). M-mode recordings were used to determine the LV end-diastolic internal diameter (LVIDd), LV end-systolic internal diameter (LVIDs), LV posterior wall thickness at the ends of diastole (LVPWd) and systole (LVPWs), and LV anterior wall thickness at the ends of diastole (LVAWd) and systole (LVAWs). LV Mass and fractional shortening (FS) were calculated with the following formulas: LV Mass $= (1.053 \times ((\mathrm{LVIDd} + \mathrm{LVPWd} + \mathrm{LVAWd})^3 - \mathrm{LVIDd}^3)) \times 0.8$ and FS $\% = (\mathrm{LVIDd} - \mathrm{LVIDs})/\mathrm{LVIDd}$, respectively.

Histological analysis. Hearts from TG mice and their NTG littermates were arrested in diastole, fixed in 4% paraformaldehyde buffered with phosphate-buffered saline (PBS), routinely dehydrated, embedded in paraffin, and cut into 5 μM sections. Paraffin sections were stained with hematoxylin and eosin for routine histological analysis, and Masson's trichrome stain was used to detect collagen deposition.

Apoptosis analysis. TUNEL (terminal deoxynucleotidyltransferase dUTP nick end-labeling) staining was performed using the ApopTag Peroxidase *In Situ* Apoptosis Detection Kit (Merck Millipore, Billerica, MA, USA), according to the

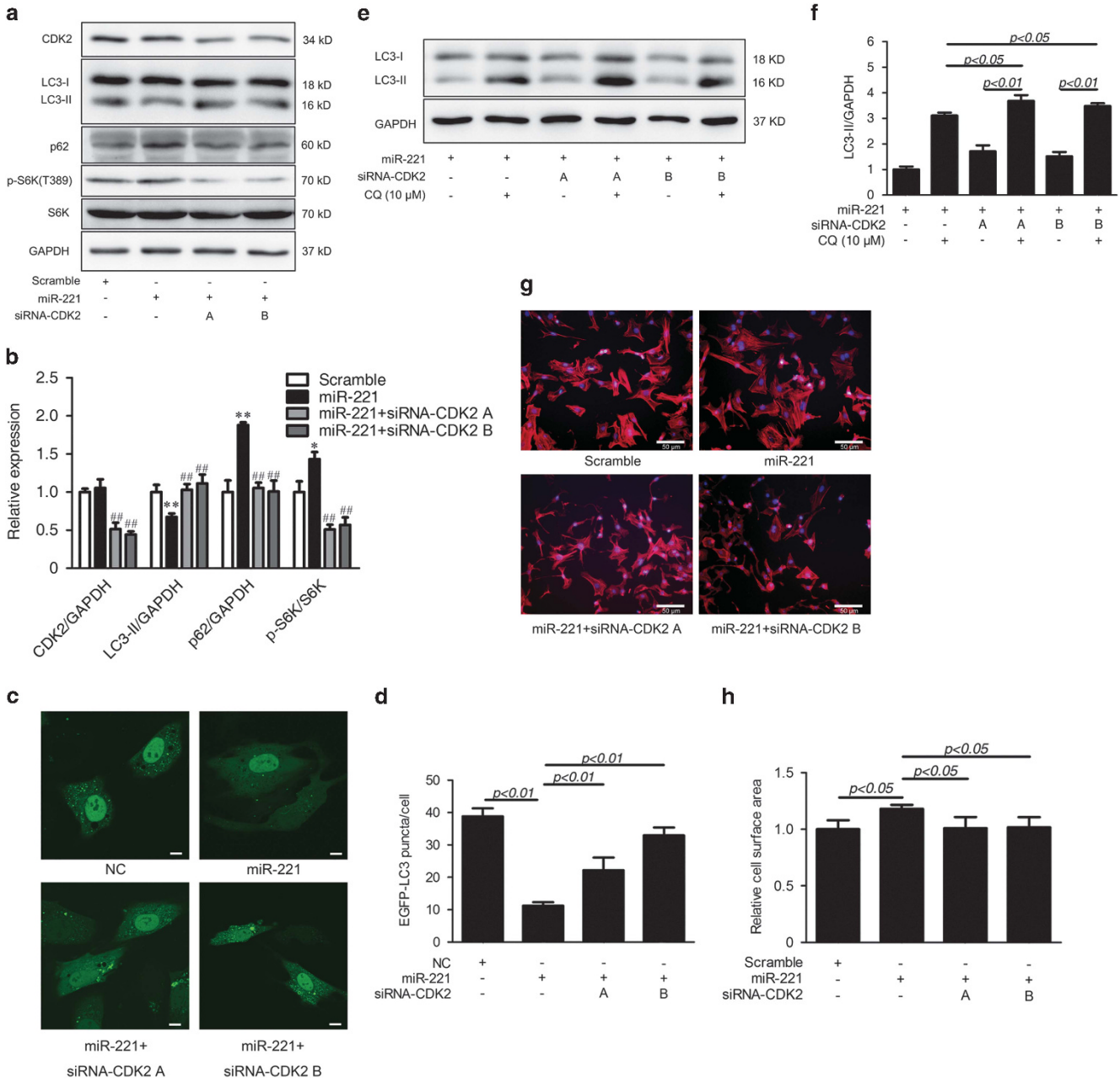

Figure 7 CDK2 knockdown attenuates miR-221-induced autophagy inhibition and cardiac hypertrophy. (**a** and **b**) CDK2 knockdown restored miR-221-induced autophagy inhibition. H9c2 cells transfected as indicated. The phosphorylation status of S6K and levels of LC3-II and p62 are shown (**a**) and quantified (**b**). $^{*}P<0.01$ and $^{**}P<0.01$ compared with the scramble group and $^{\#\#}P<0.01$ compared with the miR-221 group. (**c** and **d**) H9c2 cells transiently expressing EGFP-LC3 were co-transfected with miR-221 mimics or scramble together with two siRNAs targeting CDK2, as indicated. Representative images (**c**) and quantification (**d**) of EGFP-LC3 puncta (green) are shown. Scale bars: 10 μM. (**e**, **f**) CDK2 knockdown re-activated miR-221-induced autophagic flux impairment. Western blotting images depict LC3-I and LC3-II in H9c2 cells treated as indicated (**e**). Ratios of LC3-II/GAPDH are shown (**f**). (**g** and **h**) CDK2 silencing rescues the cardiomyocyte hypertrophy induced by miR-221 overexpression. Cultured neonatal rat cardiomyocytes were transfected and treated, as indicated. F-actin and the nuclei of cultured neonatal rat cardiomyocytes were stained with Texas Red-phalloidin and DAPI, respectively. Scale bars: 50 μm (**g**). The cell surface area was quantified with Image Pro-Plus 6.0 (**h**). All of the data were obtained from at least three independent experiments and the values are expressed as the means $\pm$ S.D.

manufacturer's protocol. In brief, samples were fixed with 4% formaldehyde, embedded in paraffin, and cut into 5 μM sections. The sections were de-paraffinized with xylene and subsequently rehydrated. After blocking the endogenous peroxidase with 3% H_2O_2 in PBS for 30 min, the sections were incubated in equilibration buffer for 1 min at room temperature and subsequently incubated in a working solution of TdT enzyme containing digoxigenin-dUTP at 37 °C for 60 min. After stopping the reaction with the stop/wash buffer, the sections were incubated with anti-digoxigenin peroxidase for 30 min at room temperature. Peroxidase activity was then visualized using diaminobenzidine. The sections were counterstained with hematoxylin, dehydrated, and mounted with neutral gum. For image acquisition, microscopic observations were performed using an Olympus IX71 microscope (Tokyo, Japan).

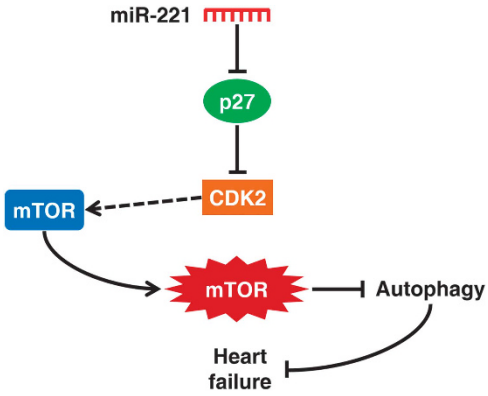

Figure 8 MiR-221 induces heart failure by inhibiting autophagy. Model depicting the downregulation of p27 expression by miR-221, resulting in CDK2-dependent mTOR activation, which inhibits autophagy to provoke heart failure

Transmission electron microscopy analysis. Myocardia were perfused and fixed in 2.5% neutral glutaraldehyde at 4 °C and post-fixed in 1% osmium tetroxide in 0.1 M sodium cacodylate buffer with 0.3% potassium ferrocyanide. Tissues in each group were stained with 4% uranyl acetate, dehydrated, infiltrated, and embedded in epoxy resin. Ultrathin sections were cut and imaged using a Hitachi H7650 transmission electron microscope (Hitachi, Tokyo, Japan).

Cell culture and treatments. Primary neonatal rat cardiomyocytes were isolated and cultured as previously described.[9] Briefly, ventricles from newborn (1-day-old) Wistar rats were washed and minced in PBS. The tissues were then digested in PBS containing 0.06% collagenase (Worthington Biochemical Corporation, Lakewood, NJ, USA) at 37 °C. After differential adhesion, the cardiomyocytes were then plated in DMEM supplemented with 10% FBS and 0.1 mM bromodeoxyuridine, and allowed to acclimate for 24 h before treatment. H9c2 cells were cultured in DMEM containing 10% FBS in an atmosphere of 5% CO_2 at 37 °C.

Cells were transiently transfected with miR-221 mimics or siRNAs using Lipofectamine 2000 reagent (Life Technologies, Carlsbad, CA, USA), according to the manufacturer's instructions. Raptor, p27, and CDK2 were respectively knocked down by using two different siRNAs, and the sequences are: Raptor A, 5′-CCCAUACAUGCCAGCUGAATT-3′ and Raptor B, 5′-GCUAGGAACCUGAACAAAUTT-3′; p27 A, 5′-CCCGGUCAAUCAUGAA GAATT-3′ and p27 B, 5′-GGCAUUUGGUGGACCAAAUTT-3′; CDK2 A, 5′-CCUC CUUAAGGAGCUCAAUTT-3′ and CDK2 B, 5′-CCAGGACCUCAAGAAGUUUTT-3′.

For p27 overexpression, the full coding sequence of human p27 was amplified with the following primers: forward: 5′-CGCGGATCCATGTCAAACGTGCGAGTGTCTA-3′; reverse: 5′-CCGGAATTCAGGATGTCCATTCCATGAAGTC-3′. The amplified fragment was cloned into the *BamH*I/*EcoR*I sites of the pcDNA3.1 vector to generate pcDNA3.1-p27 plasmid. The construct was verified by sequencing. Cells were transfected with 0.5 μg pcDNA 3.1 or pcDNA3.1-p27 plasmid with Lipofectamine 2000 reagent (Life Technologies).

For drug treatment, the cells were treated with 20 nM rapamycin (LC Laboratories, Woburn, MA, USA), or 5 or 10 μM SU9516 (Santa Cruz, Dallas, TX, USA) for 24 h. For autophagic flux analysis, cells were treated with 200 nM of rapamycin for 2 h, 100 nM of Balfilomycin A1 (Santa Cruz) for 2 h, or 10 μM of CQ (Sigma, St. Louis, MO, USA) for 1 h.

Cell surface area measurement. Primary neonatal rat cardiomyocytes were plated into 24-well plates at a density of 5×10^5 cells/ml. The cells were fixed with 4% paraformaldehyde at 48 h post transfection. The cells were then permeabilized with 1% Triton X-100 in PBS for 5 min, stained with Texas Red-phalloidin (Life Technologies) for 30 min at room temperature, and incubated with 4',6-diamidino-2-phenylindole (0.1 μg/ml) in PBS. The cell sizes in each group were assessed using a fluorescence microscope by analyzing 100 cardiomyocytes from at least 10 random fields, as described previously.[9]

Subcellular localization of EGFP-LC3 or mRFP-GFP-LC3 proteins. H9c2 cells were transfected with plasmids encoding EGFP-LC3 or mRFP-GFP-LC3 (Kimura *et al.*[46] and Kabeya *et al.*[47]), together with the corresponding small RNAs, for 48 h and were analyzed using confocal microscopy (Olympus, FV1000). The number of EGFP-LC3 puncta or GFP^+/RFP^+ (yellow) and GFP^-/RFP^+ (red) puncta per cell was quantified.

RNA extraction and quantitative RT-PCR analysis. Total RNA was isolated using the miRNeasy Mini Kit (Qiagen, Hilden, Germany). For the quantitative detection of mature miRNA, the TaqMan miRNA assay kit (Life Technologies) was used, according to the manufacturer's protocol. U6 was used to normalize the expression levels. For the quantitative detection of ANP and BNP expression levels, complementary DNAs (cDNAs) were synthesized using a cDNA synthesis kit (TaKaRa, Dalian, China). Real-time PCR was performed with specific primers: mouse ANP, 5′-AGTGCGGTGTCCAACACAG-3′ and 5′-TGCTTC CTCAGTCTGCTCACTC-3′; mouse BNP, 5′-CTTTATCTGTCACCGCTGGGAG-3′ and 5′-TTTGGGTGTTCTTTTGTGAGGC-3′; rat ANP, 5′-GGGCTCCTTCTCCAT CAC-3′ and 5′-CGGCATCTTCTCCTCCAG-3′; and rat BNP, 5′-AGAACAATCCACG ATGCAGAAG-3′ and 5′-AAACAACCTCAGCCCGTCACA-3′. GAPDH was used as a control for normalization and amplified by the following primers: mouse GAPDH, 5′-GGCATTGTGGAAGGGCTC-3′ and 5′-GGGGGTAGGAACACGGAAG-3′; and rat GAPDH, 5′-CTCTACCCACGGCAAGTTC-3′ and 5′-GCCAGTAGACTCCACGA CATA-3′.

Protein extraction and western blotting. Total protein was lysed and quantified, and 20–60 μg of protein was loaded onto SDS polyacrylamide gels for electrophoretic separation. The protein was then blotted onto a nitrocellulose membrane. Subsequently, the membrane was blocked with 5% non-fat milk or bovine serum albumin at room temperature before incubation with specific primary antibodies targeted against the following proteins: p27, p62, p-mTOR, mTOR, p-S6, S6, p-p70S6K, p70S6K, p-4E-BP1, p-ERK1/2, ERK, Bcl-2, p-AMPKα, AMPKα, p-AKT(T308), p-AKT(S473), AKT, Raptor, GAPDH (all from Cell Signaling Technology, Beverly, MA, USA), CDK2 (Santa Cruz) or LC3 (Sigma). The membrane was then incubated with HRP-conjugated secondary antibodies for 1 h at room temperature, followed by the detection of specific bands using SuperSignal West Femto Maximum Sensitivity Substrate (Pierce, Rockford, IL, USA). The band intensities were quantified with Quantity One software V4.6.2 (Bio-Rad, Hercules, CA, USA).

Statistical analysis. A two-tailed Student's *t*-test was performed using SPSS 13.0 software (SPSS Inc., Chicago, IL, USA) to determine the statistical significance of the results. $P < 0.05$ was considered statistically significant. The data are presented as the means $\pm$ S.D.

Conflict of Interest

The authors declare no conflict of interest.

Acknowledgements. We thank Dr Xuejun Jiang for kindly providing the EGFP-LC3 plasmid and Dr Tamotsu Yoshimori from Osaka University for mRFP-GFP-LC3 plasmid. This study was funded by the Ministry of Science and Technology of China (2007DFC30340, 2010CB732601, and 2011BAI11B04), and the National Natural Science Foundation of China (81070100 and 30700322).

1. Go AS, Mozaffarian D, Roger VL, Benjamin EJ, Berry JD, Borden WB *et al.* Heart disease and stroke statistics–2013 update: a report from the American Heart Association. *Circulation* 2013; **127**: e6–e245.
2. Valencia-Sanchez MA, Liu J, Hannon GJ, Parker R. Control of translation and mRNA degradation by miRNAs and siRNAs. *Genes Dev* 2006; **20**: 515–524.
3. Wang J, Huang W, Xu R, Nie Y, Cao X, Meng J *et al.* MicroRNA-24 regulates cardiac fibrosis after myocardial infarction. *J Cell Mol Med* 2012; **16**: 2150–2160.
4. Ucar A, Gupta SK, Fiedler J, Erikci E, Kardasinski M, Batkai S *et al.* The miRNA-212/132 family regulates both cardiac hypertrophy and cardiomyocyte autophagy. *Nat Commun* 2012; **3**: 1078.
5. Ge Y, Pan S, Guan D, Yin H, Fan Y, Liu J *et al.* MicroRNA-350 induces pathological heart hypertrophy by repressing both p38 and JNK pathways. *Biochim Biophys Acta* 2013; **1832**: 1–10.
6. Care A, Catalucci D, Felicetti F, Bonci D, Addario A, Gallo P *et al.* MicroRNA-133 controls cardiac hypertrophy. *Nat Med* 2007; **13**: 613–618.
7. Callis TE, Pandya K, Seok HY, Tang RH, Tatsuguchi M, Huang ZP *et al.* MicroRNA-208a is a regulator of cardiac hypertrophy and conduction in mice. *J Clin Invest* 2009; **119**: 2772–2786.
8. Ono K, Kuwabara Y, Han J. MicroRNAs and cardiovascular diseases. *FEBS J* 2011; **278**: 1619–1633.

9. Wang C, Wang S, Zhao P, Wang X, Wang J, Wang Y *et al.* MiR-221 promotes cardiac hypertrophy in vitro through the modulation of p27 expression. *J Cell Biochem* 2012; **113**: 2040–2046.
10. Levine B, Klionsky DJ. Development by self-digestion: molecular mechanisms and biological functions of autophagy. *Dev Cell* 2004; **6**: 463–477.
11. Schramm C, Fine DM, Edwards MA, Reeb AN, Krenz M. The PTPN11 loss-of-function mutation Q510E-Shp2 causes hypertrophic cardiomyopathy by dysregulating mTOR signaling. *Am J Physiol Heart Circ Physiol* 2012; **302**: H231–H243.
12. Nakai A, Yamaguchi O, Takeda T, Higuchi Y, Hikoso S, Taniike M *et al.* The role of autophagy in cardiomyocytes in the basal state and in response to hemodynamic stress. *Nat Med* 2007; **13**: 619–624.
13. Taneike M, Yamaguchi O, Nakai A, Hikoso S, Takeda T, Mizote I *et al.* Inhibition of autophagy in the heart induces age-related cardiomyopathy. *Autophagy* 2010; **6**: 600–606.
14. Matsui Y, Takagi H, Qu X, Abdellatif M, Sakoda H, Asano T *et al.* Distinct roles of autophagy in the heart during ischemia and reperfusion: roles of AMP-activated protein kinase and Beclin 1 in mediating autophagy. *Circ Res* 2007; **100**: 914–922.
15. Zhu H, Tannous P, Johnstone JL, Kong Y, Shelton JM, Richardson JA *et al.* Cardiac autophagy is a maladaptive response to hemodynamic stress. *J Clin Invest* 2007; **117**: 1782–1793.
16. Shih H, Lee B, Lee RJ, Boyle AJ. The aging heart and post-infarction left ventricular remodeling. *J Am Coll Cardiol* 2011; **57**: 9–17.
17. Hara K, Maruki Y, Long X, Yoshino K, Oshiro N, Hidayat S *et al.* Raptor, a binding partner of target of rapamycin (TOR), mediates TOR action. *Cell* 2002; **110**: 177–189.
18. Shende P, Plaisance I, Morandi C, Pellieux C, Berthonneche C, Zorzato F *et al.* Cardiac raptor ablation impairs adaptive hypertrophy, alters metabolic gene expression, and causes heart failure in mice. *Circulation* 2011; **123**: 1073–1082.
19. Bodine SC, Stitt TN, Gonzalez M, Kline WO, Stover GL, Bauerlein R *et al.* Akt/mTOR pathway is a crucial regulator of skeletal muscle hypertrophy and can prevent muscle atrophy in vivo. *Nat Cell Biol* 2001; **3**: 1014–1019.
20. Appenzeller-Herzog C, Hall MN. Bidirectional crosstalk between endoplasmic reticulum stress and mTOR signaling. *Trends Cell Biol* 2012; **22**: 274–282.
21. Shaw RJ, Bardeesy N, Manning BD, Lopez L, Kosmatka M, DePinho RA *et al.* The LKB1 tumor suppressor negatively regulates mTOR signaling. *Cancer cell* 2004; **6**: 91–99.
22. Ma L, Chen Z, Erdjument-Bromage H, Tempst P, Pandolfi PP. Phosphorylation and functional inactivation of TSC2 by Erk implications for tuberous sclerosis and cancer pathogenesis. *Cell* 2005; **121**: 179–193.
23. Liang J, Shao SH, Xu ZX, Hennessy B, Ding Z, Larrea M *et al.* The energy sensing LKB1-AMPK pathway regulates p27(kip1) phosphorylation mediating the decision to enter autophagy or apoptosis. *Nat Cell Biol* 2007; **9**: 218–224.
24. Jiang H, Martin V, Gomez-Manzano C, Johnson DG, Alonso M, White E *et al.* The RB-E2F1 pathway regulates autophagy. *Cancer Res* 2010; **70**: 7882–7893.
25. Toyoshima H, Hunter T. p27, a novel inhibitor of G1 cyclin-Cdk protein kinase activity, is related to p21. *Cell* 1994; **78**: 67–74.
26. Polyak K, Kato JY, Solomon MJ, Sherr CJ, Massague J, Roberts JM *et al.* p27Kip1, a cyclin-Cdk inhibitor, links transforming growth factor-beta and contact inhibition to cell cycle arrest. *Genes Dev* 1994; **8**: 9–22.
27. Tamamori-Adachi M, Hayashida K, Nobori K, Omizu C, Yamada K, Sakamoto N *et al.* Down-regulation of p27Kip1 promotes cell proliferation of rat neonatal cardiomyocytes induced by nuclear expression of cyclin D1 and CDK4. Evidence for impaired Skp2-dependent degradation of p27 in terminal differentiation. *J Biol Chem* 2004; **279**: 50429–50436.
28. Thomas RL, Roberts DJ, Kubli DA, Lee Y, Quinsay MN, Owens JB *et al.* Loss of MCL-1 leads to impaired autophagy and rapid development of heart failure. *Genes Dev* 2013; **27**: 1365–1377.
29. Ceylan-Isik AF, Dong M, Zhang Y, Dong F, Turdi S, Nair S *et al.* Cardiomyocyte-specific deletion of endothelin receptor A rescues aging-associated cardiac hypertrophy and contractile dysfunction: role of autophagy. *Basic Res Cardiol* 2013; **108**: 335.
30. Kim J, Kundu M, Viollet B, Guan KL. AMPK and mTOR regulate autophagy through direct phosphorylation of Ulk1. *Nat Cell Biol* 2011; **13**: 132–141.
31. Zhang D, Contu R, Latronico MV, Zhang J, Rizzi R, Catalucci D *et al.* MTORC1 regulates cardiac function and myocyte survival through 4E-BP1 inhibition in mice. *J Clin Invest* 2010; **120**: 2805–2816.
32. Ramos FJ, Chen SC, Garelick MG, Dai DF, Liao CY, Schreiber KH *et al.* Rapamycin reverses elevated mTORC1 signaling in lamin A/C-deficient mice, rescues cardiac and skeletal muscle function, and extends survival. *Sci Transl Med* 2012; **4**: 144ra103.
33. Choi JC, Muchir A, Wu W, Iwata S, Homma S, Morrow JP *et al.* Temsirolimus activates autophagy and ameliorates cardiomyopathy caused by lamin A/C gene mutation. *Sci Transl Med* 2012; **4**: 144ra102.
34. Marin TM, Keith K, Davies B, Conner DA, Guha P, Kalaitzidis D *et al.* Rapamycin reverses hypertrophic cardiomyopathy in a mouse model of LEOPARD syndrome-associated PTPN11 mutation. *J Clin Invest* 2011; **121**: 1026–1043.
35. Petiot A, Ogier-Denis E, Blommaart EF, Meijer AJ, Codogno P. Distinct classes of phosphatidylinositol 3'-kinases are involved in signaling pathways that control macroautophagy in HT-29 cells. *J Biol Chem* 2000; **275**: 992–998.
36. Memmott RM, Dennis PA. Akt-dependent and -independent mechanisms of mTOR regulation in cancer. *Cell Signal* 2009; **21**: 656–664.
37. Inoki K, Zhu T, Guan KL. TSC2 mediates cellular energy response to control cell growth and survival. *Cell* 2003; **115**: 577–590.
38. Gwinn DM, Shackelford DB, Egan DF, Mihaylova MM, Mery A, Vasquez DS *et al.* AMPK phosphorylation of raptor mediates a metabolic checkpoint. *Mol Cell* 2008; **30**: 214–226.
39. Wang RH, Kim HS, Xiao C, Xu X, Gavrilova O, Deng CX. Hepatic Sirt1 deficiency in mice impairs mTorc2/Akt signaling and results in hyperglycemia, oxidative damage, and insulin resistance. *J Clim Invest* 2011; **121**: 4477–4490.
40. Li JM, Brooks G. Downregulation of cyclin-dependent kinase inhibitors p21 and p27 in pressure-overload hypertrophy. *Am J Physiol* 1997; **273**(3 Pt 2): H1358–H1367.
41. Burton PB, Yacoub MH, Barton PJ. Cyclin-dependent kinase inhibitor expression in human heart failure. A comparison with fetal development. *Eur Heart J* 1999; **20**: 604–611.
42. Hauck L, Harms C, An J, Rohne J, Gertz K, Dietz R *et al.* Protein kinase CK2 links extracellular growth factor signaling with the control of p27(Kip1) stability in the heart. *Nat Med* 2008; **14**: 315–324.
43. Sun X, Momen A, Wu J, Noyan H, Li R, von Harsdorf R *et al.* p27 Protein protects metabolically stressed cardiomyocytes from apoptosis by promoting autophagy. *J Biol Chem* 2014; **289**: 16924–16935.
44. National Academies Press (US)*The National Academies Collection: Reports funded by National Institutes of Health. Guide for the Care and Use of Laboratory Animals*8th ednNational Academies Press (US): Washington (DC), 2011.
45. Wang X, Wang J, Su M, Wang C, Chen J, Wang H *et al.* TNNI3K, a cardiac-specific kinase, promotes physiological cardiac hypertrophy in transgenic mice. *PLoS ONE* 2013; **8**: e58570.
46. Kimura S, Noda T, Yoshimori T. Dissection of the autophagosome maturation process by a novel reporter protein, tandem fluorescent-tagged LC3. *Autophagy* 2007; **3**: 452–460.
47. Kabeya Y, Mizushima N, Ueno T, Yamamoto A, Kirisako T, Noda T *et al.* LC3, a mammalian homologue of yeast Apg8p, is localized in autophagosome membranes after processing. *EMBO J* 2000; **19**: 5720–5728.

Supplementary Information accompanies this paper on Cell Death and Differentiation website (http://www.nature.com/cdd)